Los Alamos NATIONAL LABORATORY EST.1943

LA-UR-20-28112 (Accepted Manuscript)

Association Between EMIC Wave Occurrence and Enhanced Convection Periods During Ion Injections

Remya, B.
Sibeck, David G.
Ruohoniemi, J. M.
Kundrui, B.
Halford, A. J.
Reeves, Edmond Geoffrey David
Reddy, R. V.

Provided by the author(s) and the Los Alamos National Laboratory (2021-01-13).

To be published in: Geophysical Research Letters

DOI to publisher's version: 10.1029/2019GL085676

Permalink to record: http://permalink.lanl.gov/object/view?what=info:lanl-repo/lareport/LA-UR-20-28112

Disclaimer:
Los Alamos National Laboratory, an affirmative action/equal opportunity employer, is operated by Triad National Security, LLC for the National Nuclear Security Administration of U.S. Department of Energy under contract 89233218CNA000001. By approving this article, the publisher recognizes that the U.S. Government retains nonexclusive, royalty-free license to publish or reproduce the published form of this contribution, or to allow others to do so, for U.S. Government purposes. Los Alamos National Laboratory requests that the publisher identify this article as work performed under the auspices of the U.S. Department of Energy. Los Alamos National Laboratory strongly supports academic freedom and a researcher's right to publish; as an institution, however, the Laboratory does not endorse the viewpoint of a publication or guarantee its technical correctness.

RESEARCH LIBRARY

Association between EMIC wave occurrence and enhanced convection periods during ion injections

B. Remya[1], D.G. Sibeck[2], J.M. Ruohoniemi[3], B. Kunduri[3], A.J. Halford[4], G. D. Reeves[5], and R. V. Reddy[1]

[1]Indian Institute of Geomagnetism, Navi Mumbai, India.
[2]NASA Goddard Space Flight Center, Maryland, USA.
[3]Center For Space Science and Engineering Research, Virginia Tech, Blacksburg, Virginia, USA.
[4]The Aerospace Corporation, Space Sciences Department, Chantilly, USA.
[5]Los Alamos National Laboratory, Los Alamos, New Mexico, USA.

Key Points:

- Ion injection triggered EMIC waves with no influence from geomagnetic storms or solar wind pressure pulses are reported
- Enhanced ionospheric convection periods are associated with substorm injection triggered EMIC waves
- Ionospheric convection periods are direct evidence for the associated enhanced magnetospheric convection during injections

Corresponding author: Remya Bhanu, remyaphysics@gmail.com

Abstract

Electromagnetic ion cyclotron (EMIC) waves tend to occur during geomagnetic storms and solar wind pressure pulses. However, they have also been regularly observed even in the absence of these two drivers. These non-storm time and non-pressure pulse EMIC events are very well associated with individual night side injections (Remya et al., 2018). Nevertheless, not all substorm injections elicit wave activity. We examine the EMIC events excited during two substorm injections on 4 September 2015 and 1 October 2015. We find that injections that are associated with EMIC waves are also associated with enhanced ionospheric convection. The convective signatures occur at local times similar to those of the observed wave activity.

Plain Language Summary

Geomagnetic storms and magnetospheric compressions owing to solar wind pressure pulses are considered to be the two major drivers for electromagnetic ion cyclotron (EMIC) waves in the Earth's magnetosphere. However, it is found that substorms act as a major free energy source for these waves in the absence of geomagnetic storms or solar wind pressure pulses. In this study, we identify such non-storm time non-pressure pulse driven EMIC waves and find that they are very well associated with substorm injections. We find direct evidence of correspondence of these injection driven waves with enhanced ionospheric convection which are manifestation of enhanced magnetospheric electric fields.

1 Introduction

The interplanetary magnetic field (IMF) plays a crucial role in driving the dynamics of the terrestrial magnetosphere. The solar wind magnetic field reconnects with the geomagnetic field enabling plasma, momentum and energy to enter the magnetosphere and inducing large-scale convection of magnetospheric plasma (Dungey, 1961). This Dungey convection cycle comprises a general antisunward transport of open flux from the subsolar magnetopause over the polar caps and a sunward return flow of closed flux in the magnetotail and inner magnetosphere due to night side reconnection. Dayside and nightside reconnection can occur independently. Large scale magnetospheric convection generates convection electric fields which map along the geomagnetic field lines to the high latitude ionosphere. In response to these electric fields of magnetospheric origin, the high latitude ionospheric plasma convects with a velocity $\vec{v} = \vec{E} \times \vec{B}/B^2$, where $\vec{E}$ is the ionospheric electric field and $\vec{B}$ is the geomagnetic field.

The flux transport activity varies with varying IMF conditions (Rossberg, 1984; Cowley & Lockwood, 1992; Ruohoniemi et al., 2002; Milan, 2015). The response of high latitude convection to varying IMF conditions on the dayside is understood near simultaneous at all MLTs extending from noon to midnight occurring within a very short (2-8 mins) time span (Ruohoniemi & Greenwald, 1998; Khan & Cowley, 1999; Shepherd et al., 1999). However, it is less clear how rapidly global convection responds to the onset of night side reconnection.

One of the phenomena that initiates this flux and energy transport is a substorm. Substorms occur, on an average, four times a day (Borovsky et al., 1993). They are more frequent and more intense during geomagnetic storms. The night side injections during substorms transport energetic ions and electrons of energies 1-100 keVs from the plasma sheet in to the inner magnetosphere (Axford, 1969). Even in the absence of substorms, such transport occurs during localized particle injections resulting from plasma sheet flow bursts resulting in sudden particle flux enhancements (Baker et al., 1978; Birn et al., 1997; Denton et al., 2016). All these injections induce a temperature anisotropy by adiabatically heating the plasma (Cornwall & Schulz, 1971), thereby producing conditions un-

stable to electromagnetic cyclotron waves (Cornwall, 1965). While injections drive chorus waves by resonance with electrons, in the dawn or post-midnight sector (Li et al., 2009), electromagnetic ion cyclotron (EMIC) waves occur primarily in the dusk or pre-midnight sector (Halford et al., 2016). The dawn/dusk dominance of these waves is due to the charge dependence of the particle drift in the Earth's gradient magnetic field.

Understanding generation mechanisms for EMIC waves (0.1-5 Hz), has been of great research interest as they act as an important loss process for both ring current ions and radiation belt electrons [(Kennel & Petschek, 1966; Thorne & Kennel, 1971; Jordanova et al., 2008) and references therein]. It is well known that geomagnetic activity favors EMIC wave growth. The occurrence of EMIC waves during different phases of geomagnetic storms has been investigated by many, for example, Erlandson and Ukhorskiy (2001); Engebretson et al. (2008); Halford et al. (2010); Wang et al. (2016) and references therein. Non-storm time and quiet time EMIC events have also been explored in detail (Anderson & Hamilton, 1993; Engebretson et al., 2015; Park et al., 2016; Halford et al., 2016) and are mostly found to be associated with compressions of the dayside magnetosphere due to solar wind pressure pulses (Olson & Lee, 1983). A third important source of free energy that nurtures EMIC wave growth is substorm injections. These injections could be during storm time substorms, isolated non-storm time substorms or localized particle injections resulting from plasma sheet flow bursts. The role of substorm injections in triggering EMIC waves has been dealt in detail by Remya et al. (2018) who presented a case study of an isolated substorm on 09 August 2015. The arrival of hot ion injections along with an associated decrease in the geomagnetic field strength and enhanced temperature anisotropy favor the growth of EMIC waves. The present paper focuses on similar EMIC wave events that are triggered solely due to substorm-injected ions, with no influence from geomagnetic storms or enhancements in solar wind dynamic pressure, ensuring that the source for EMIC wave free energy during non-storm intervals is only the anisotropic ion injections on the nightside. This paper seeks to determine which substorm injections favor EMIC wave growth.

Hwang et al. (2007) showed that dawn side chorus waves are associated with enhanced convection. Their statistical study suggests that it is the periods of enhanced convection that precede substorm expansions and not the expansions themselves that lead to the enhanced dawn side chorus wave intensity. The present study identifies a similar association for injection triggered EMIC waves in the Earth's magnetosphere. We surveyed ion injection triggered EMIC waves from January 2013 to December 2015 during the Van Allen Probes (VAP) era. Most events showed signatures of strong magnetospheric plasma convection associated with the EMIC wave enhancements. We further validated the results by inspecting events with and without EMIC waves during a two-month period (September-October 2015) with a total of 134 injection events. These two months were selected as spacecraft apogees were on the dusk side, the region where EMIC waves are most likely to occur. Injection events with associated EMIC waves are associated with signatures of strong convection surges. In this letter, we report evidence for strong convection surges associated with ion injection triggered EMIC waves. To put the observations into context we show two representative cases demonstrating the association of strong convection to ion injection triggered EMIC waves.

2 Observations

2.1 Ion Injections and EMIC Waves

Figure 1a- 1e shows magnetic field, EMIC wave and particle data during the interval 00:00-04:00 UT for the first event on 04 September 2015 (satellite trajectories are shown in Figure S1a in supporting information(SI)). The left-hand and right-hand side plots are for the twin Van Allen Probes, VAP-A and VAP-B, respectively. These spacecraft have highly elliptical orbits with an apogee of 5.8 R_E and were in the dusk sector

during this study interval. Panels 1a1 and 1a2 show time variation of the magnetic field components in the GSE coordinate system. In panel 1a1, fluctuations in the B_x component are clearly seen for VAP-A with a small decrease around ∼01:36 UT. As the spacecraft was approaching its perigee, the field values are quite high and the fluctuations are not clearly visible in other components. At VAP-B (Figure 1a2), fluctuations in all magnetic field components are noticeable starting approximately around ∼01:30 until 03:20 UT. Figure 1b1 and 1b2 show dynamic spectra of the high resolution (64 samples/s) magnetic field data from the EMFISIS triaxial fluxgate magnetometer (Kletzing et al., 2013). The white lines are the cyclotron frequencies of proton (solid), Helium (dashed), and Oxygen (dash-dotted line). VAP-A observes EMIC waves in the Oxygen band at ∼01:36 UT and the frequencies spread to the Helium branch shortly thereafter. Strong EMIC waves in the Helium branch occur after 02:00UT. At ∼02:30 UT, intense EMIC waves occur in the Helium band and further spread in frequencies to the Hydrogen band. Strong fluctuations below the Oxygen cyclotron frequency overlay broadband fluctuations before ∼01:30 UT which may be the Oxygen band EMIC waves. In Figure 1b2, strong Helium band EMIC waves occur sporadically at VAP-B with onsets at ∼01:33 UT, ∼01:44 UT, ∼03:24 UT, and ∼03:43 UT.

Figure 1c1 and 1c2 show spin averaged proton fluxes from RBSPICE (Mitchell et al., 2013) and ECT/HOPE (Spence et al., 2013; Funsten et al., 2013) instruments. Panels 1d1 and 1d2 shows SOPA ion fluxes from a single LANL (Reeves et al., 1996) spacecraft which was located westward of midnight during respective events so that the ion flux enhancements at geosynchronous orbits, if any, are clearly visible. The vertical solid black lines in both the left- and right-hand panels indicate the times of ion flux increases at ∼00:04 UT, ∼01:33 UT, ∼02:29 UT, and ∼03:40 UT, respectively, observed at any of RBSPICE/HOPE/LANL spacecraft. Sudden flux increases observed at LANL, RBSPICE and/or HOPE at ∼01:33 UT and ∼02:29 UT at VAP-A and at ∼01:33 UT and ∼03:40 UT at VAP-B are well associated with EMIC wave enhancements at the respective spacecraft. The flux increases in the higher energy channels are clearly visible in the pitch angle (PA) resolved plots from RBSPICE and HOPE (Figure S2 in SI). The substorm list from the SuperMAG database (Newell & Gjerloev, 2011a, 2011b) shows substorm onsets corresponding to the events of study. Table S1 of the supporting information tabulates list of substorms for the two study intervals. The grey dashed vertical line in Figure 1 indicates an official substorm onset time at 03:30 UT on 04 September 2015 as obtained from SuperMAG database. Another onset time from the list is at 23:05 UT on the previous day (03 September 2015), which is probably the substorm associated with our event (not shown on the plot). Panels 1e1 and 1e2 show variations in AE index during the event. The AE index is >350 nT throughout the interval, increases to 643 nT just before the flux enhancement at ∼01:33 UT and later on peaks at 915 nT at 04:00 UT.

Figure 2 displays plots similar to those in Figure 1 for two EMIC events observed by VAP- A during the interval 14:00-18:00 UT (left-hand panels) and VAP-B during 21:00-24:00 UT (right-hand panels) on 01 October 2015 (refer to Figure S1b for satellite orbits). We will discuss the events one by one. In Figure 2a1, the magnetic field fluctuations are clearly seen starting at ∼15:43 UT. Figure 2b1 shows strong Helium band EMIC waves starting at ∼15:43 UT which extends for more than one hour until 17:00 UT. The flux variations from VAP-A and LANL-02A (located close to midnight) shown in Figure 2c1 and 2d1, respectively, indicate sudden rise in ion fluxes at ∼15:43 UT (black solid vertical line) corresponding to the EMIC wave onset at VAP-A. The flux rise is discernible in LANL, HOPE energy channels and lower energy channels from RBSPICE. For a more pronounced picture, the reader may refer to PA resolved plots in Figure S3 in the SI. The other probe VAP-B was in its inbound trajectory at $L \simeq 3$ during this interval and only sees a weak patch of EMIC wave at ∼15:05 UT (not shown). Figure 2e1 shows disturbed geomagnetic conditions during the event with AE index increasing to 885 nT at ∼15:55 UT. Substorm onset times from Table S1 marked as grey dashed vertical lines show on-

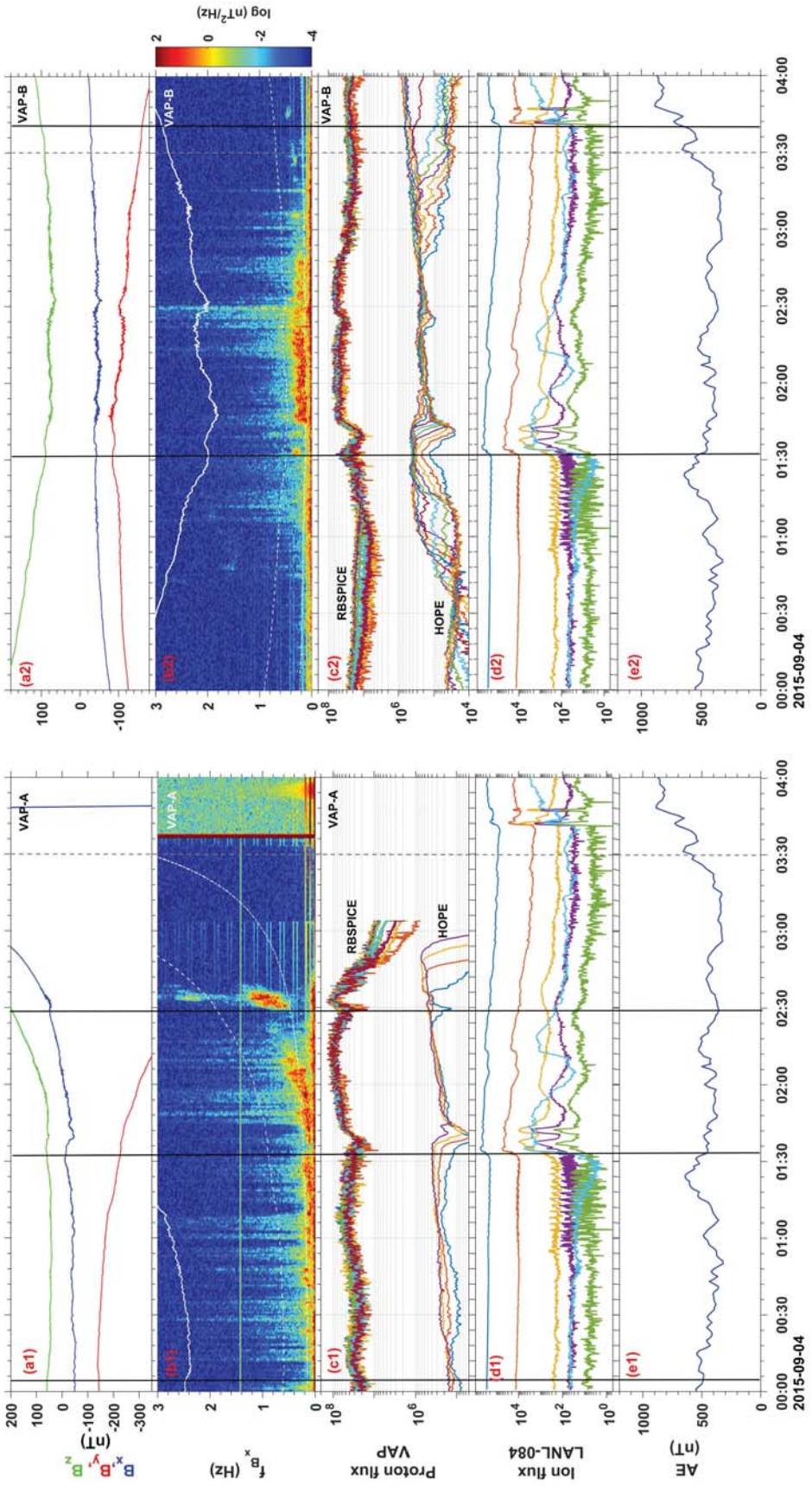

Figure 1. Time variation of the magnetic field components in GSE coordinates from (a1) VAP-A and (a2) VAP-B during 00:00-04:00 UT on 04 September 2015. (b1 and b2) Dynamic spectra of magnetic field B_x component. White lines indicate the gyrofrequencies for proton (solid), Helium (dashed) and Oxygen (dash-dotted). (c1 and c2) Time variation of the spin averaged proton flux observed by RBSPICE (50-600 keV) and HOPE (10-51 keV) instruments. (d1 and d2) LANL SOPA ion fluxes from 75 keV to 1.2 MeV from LANL-084 geosynchronous spacecraft and (e1 and e2) AE index. The black solid vertical lines indicate approximate start times of injections in each probe. Grey dashed vertical lines indicate substorm onset times during the interval from Table S1.

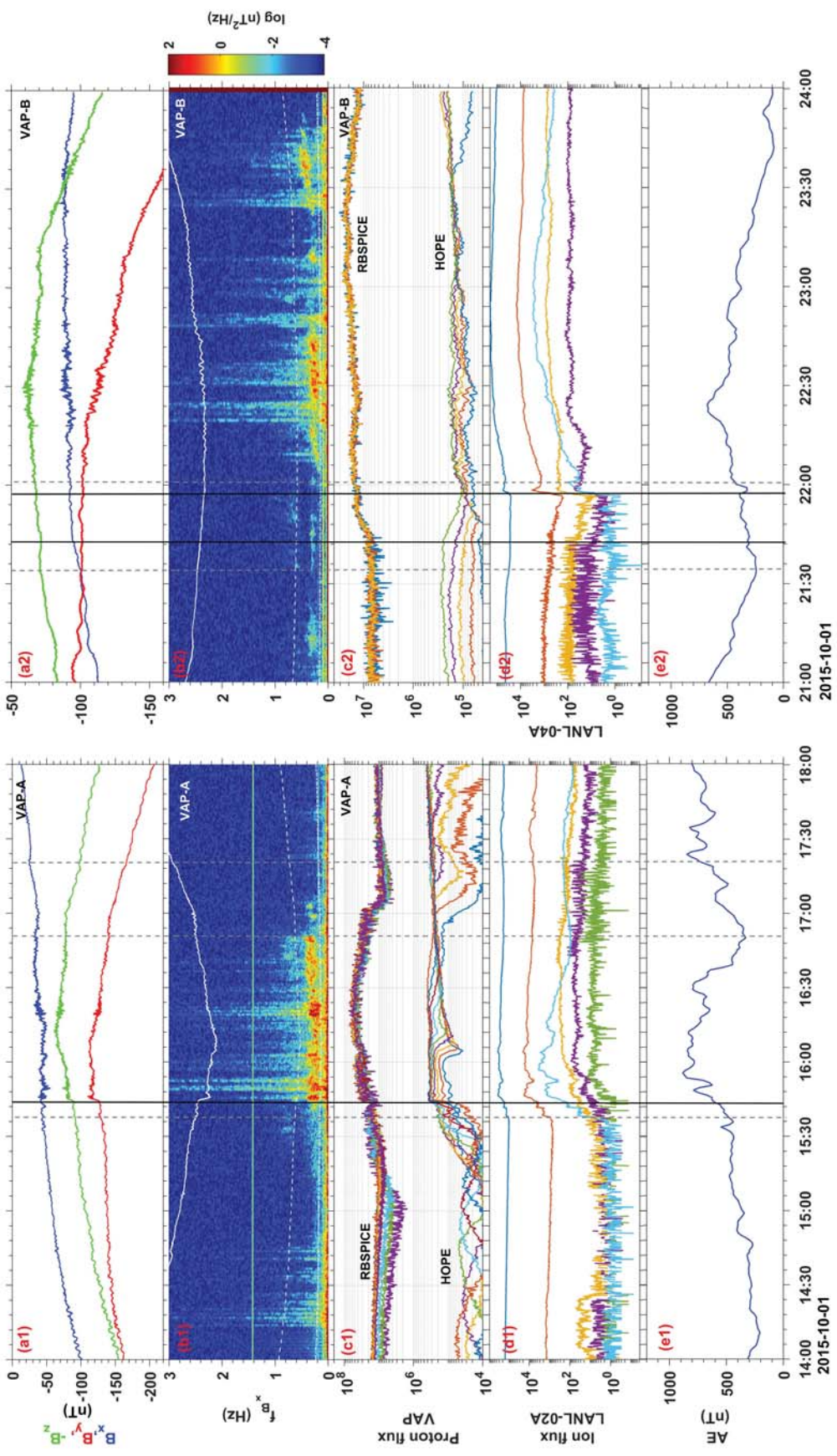

Figure 2. Time variation of the magnetic field components in GSE coordinates during (a1) 14:00-18:00 UT from VAP-A and (a2) 21:00-24:00 UT from VAP-B on 01 October 2015. (b1 and b2) Respective dynamic spectra of magnetic field B_x component (c1 and c2) Time variation of the spin averaged proton flux observed by RBSPICE (50-600 keV) and HOPE (10-51 keV) instruments. LANL SOPA ion fluxes from 75 keV to 1.2 MeV from (d1) LANL-02A and (d2) LANL-04A geosynchronous spacecraft and (e1 and e2) AE index. The black solid vertical lines indicate approximate start times of injections in each probe. Grey dashed vertical lines indicate substorm onset times during the interval from Table S1.

sets at ∼15:37 UT, ∼16:51 UT, and ∼17:20 UT on 01 October 2015. The onset at ∼15:37 UT well corresponds to the injection and EMIC onset at ∼15:43 UT.

More EMIC wave events occur sporadically later on the day at VAP-B (Figure 2b2) with onsets at ∼21:08 UT, ∼21:34 UT, ∼22:04 UT, ∼23:06 UT, and ∼23:22 UT. The magnetic field fluctuations are seen in Figure 2a2. The flux plots in Figures 2c2 and 2d2 show flux increases at ∼21:43 UT on VAP-B and at ∼21:57 UT on LANL-04A. These signatures are closely associated with EMIC wave patches at ∼21:34 UT, and ∼22:04 UT. No clear flux rise is observed corresponding to other EMIC wave patches. The flux increases do not seem to be very intense in the PA resolved plots (Figure S3) either. Figure 2e2 indicate disturbed conditions with AE gradually increasing during the event and peaks to 669 nT at ∼22:25 UT. The substorm list in Table S1 shows substorm onset times at 21:34 UT and 22 :02 UT which are well associated with the flux rise and corresponding EMIC wave onset times at ∼21:34 UT and ∼22:04 UT, respectively.

2.2 Solar Wind and Geomagnetic conditions

Our study addresses substorm ion injection triggered EMIC waves in the absence of a geomagnetic storm or solar wind pressure pulses. Figure 3 gives the solar wind parameters and geomagnetic indices during these 2 events to confirm this. The solar wind parameters and geomagnetic indices are obtained from the NASA/GSFC's OMNI database. The solar wind observations are time shifted to the nose of Earth's bowshock. The left- and right-hand panels are for days (i) 04 September 2015 and (ii) 01 October 2015, respectively. The panels from top to bottom are (a) IMF B_z, (b) solar wind speed, (c) solar wind dynamic pressure, (d) AE, and (e) SYM-H. The vertical black solid lines mark the start time of the injections or flux rises from corresponding Figures 1 and 2.

For the first event on 04 September 2015, the IMF B_z stays southward (∼-10 nT) for $>$ 2hrs before the EMIC wave onset and turns northward later. Lee et al. (2006) showed that a northward turning of Alfvénic IMF fluctuations preceded by a moderately southward IMF B_z leads to a significant fraction of substorm onsets which is also what we see here. The AE index is enhanced (643 nT at EMIC wave onset ∼01:33 UT) and peaks later near 915 nT at 04:00 UT. The SYM-H index corresponds to a non-storm time interval (minimum of -39 nT). The second event on 01 October 2015 has similar geomagnetic and solar wind conditions with increased AE activity (∼883 nT), minimum SYM-H index of ∼-31 nT (non-storm time), and prolonged southward IMF B_z interval since ∼2 hrs before the start of EMIC waves. The solar wind dynamic pressure ($\simeq$4 nPa) does not show any drastic changes during either of the events. The flow velocities gradually increase during the wave activity periods in both events. The injection events in the present study are hence considered to be purely substorm related with no effects from geomagnetic storms or solar wind pressure pulses. The substorm list from the SuperMAG database (Table S1) also confirms substorm onsets corresponding to the events of study. The inference is further confirmed by auroral outburst observations from timely flux enhancements at geosynchronous spacecraft LANL and THEMIS All Sky Imager (ASI) (not shown due to space constraints).

2.3 SuperDARN measurements

The SuperDARN network is an international chain of radars proving coverage across the polar-, high- and mid-latitude regions in both Northern and Southern hemispheres (Greenwald et al., 1985; Chisham et al., 2007; Nishitani et al., 2019). These radars observe coherent backscatter from decameter-scale irregularities aligned along the geomagnetic field and the Doppler shift of the backscattered signal is proportional to the Line-of-Sight (L-o-S) component of the ExB plasma drift in the scattering region (Ruohoniemi et al., 1987). The measurements from several SuperDARN radars can be combined with a background statistical model using the fitting procedure described in (Ruohoniemi &

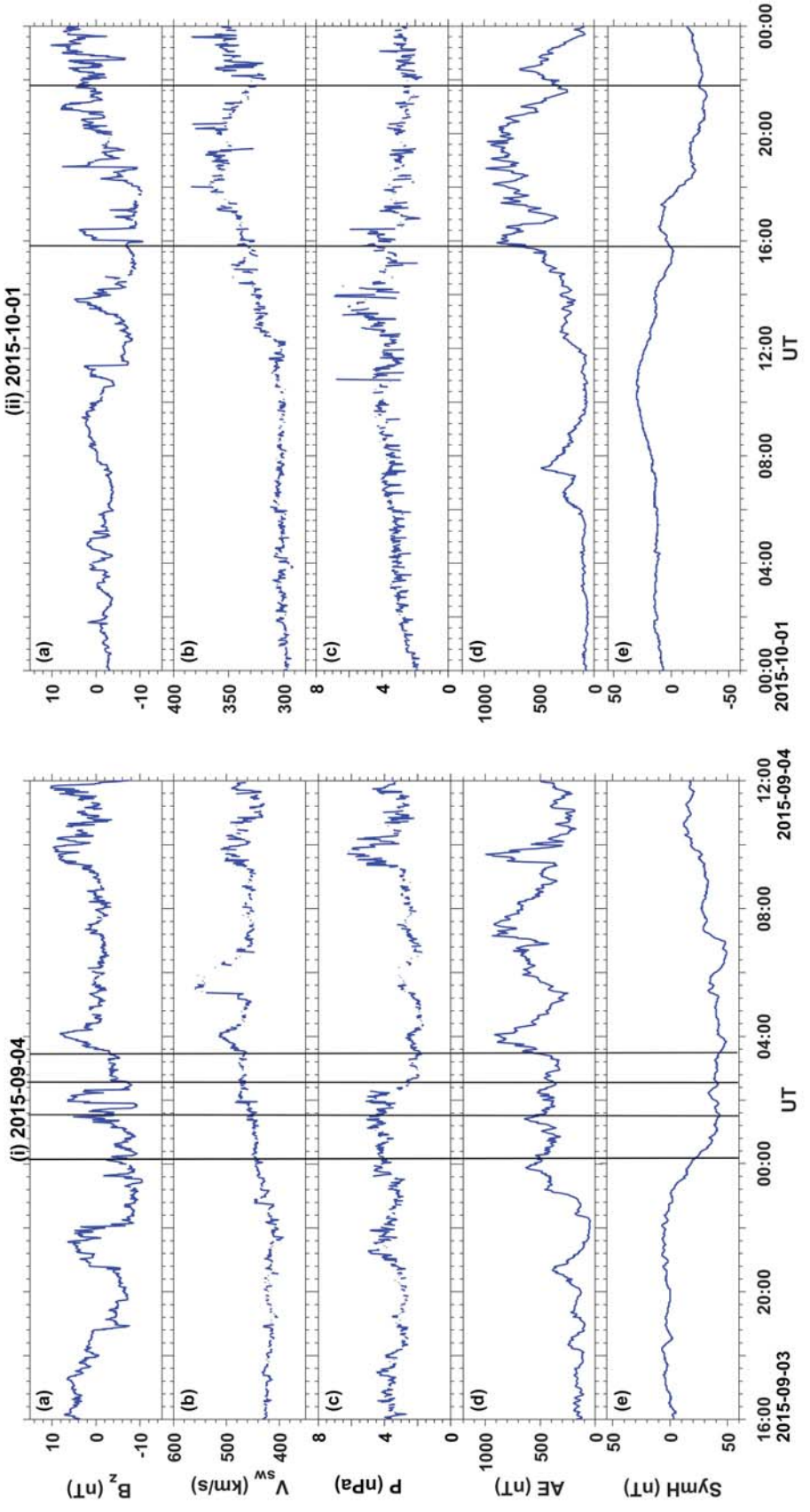

Figure 3. (a) IMF B_z (b) solar wind speed (c) solar wind dynamic pressure (d) AE and (e) SYM-H during (i) 04 September 2015 and (ii) 01 October 2015. The black vertical lines are the start time of the injections (same as in Figures 1 and 2, respectively).

Baker, 1998) to derive large scale ionospheric convection patterns. In this study we work with the line-of-sight (LOS) velocity measurements from the individual radars after mapping into the equal-area, 1-deg-in-latitude grid cells defined by Ruohoniemi and Baker (1998), which is a preliminary step for carrying out the fitting procedure. We examine these gridded LOS velocity measurements for direct evidence of convection velocity surges. This approach is preferable to working with fitted global velocity data as the spatial filtering associated with the fitting is likely to suppress the occurrence of localized velocity features. These plasma flows measured in the ionosphere is a good measure of the magnetospheric electric fields assuming that field aligned potential drops are negligible.

Figure 4 presents scatter plots of the gridded L-o-S velocity measurements (Ruohoniemi & Baker, 1998) from various radars in the northern hemisphere SuperDARN array for different magnetic latitudes (MLATs) and magnetic local times (MLTs). Each panel combines radar measurements within different fields of view that span a 4° MLAT and 3 hours MLT bins with a total latitudinal coverage of 64−76° MLAT and local time sectors from 15 to 24 MLT. The MLAT and MLT bins are noted in each panel and the legends indicate the radars that contribute to the data points in each panel.

Figure 4(a) shows the gridded L-o-S velocity magnitude measured in m/s for the event interval 00:00-04:00 UT on 04 September 2015. Enhanced magnetospheric convection associated with substorm injections are manifested as plasma convection in the ionosphere. The peak L-o-S velocity increases beyond 1250 m/s after ∼00:30 UT in the post-noon 15-18 MLT bin between 64−72° MLAT. At this time, both VAP spacecraft were located in this MLT sector during which they observed injection signatures as well as associated EMIC waves around ∼01:33 UT. On a convection map (Movie S1), these velocities are seen as a strong sunward drift of plasma which indicates return flow of the magnetic flux closed by night side reconnection to the dayside during substorms. The peak L-o-S velocities remains close to 1000 m/s in this MLT-MLAT bin until 02:20 UT and wanes below 750 m/s later. Peak L-o-S velocities of <750 m/s are seen at 18-21 MLT sector for 64 − 72° MLAT. No or weak convection surges are observed at higher latitudes (72-76° MLAT) and for 21-24 MLT regions. Velocity measurements were further checked for later hours and for the same hours on days prior and after the event (±1 day). There were no strong plasma convection signatures measured during corresponding time intervals on days prior to and after this event (not shown).

Figure 4(b) displays the L-o-S velocity scatter plot measurements for the second event on 01 October 2015 from 14:00-24:00 UT. It is very interesting to note that peak L-o-S velocities significantly rise to ∼1500 m/s during the period when injection associated EMIC waves are observed at ∼15:40 UT. This enhanced convection is observed at latitudes from 64-76° and in the post-noon 15-18 MLT sector where the spacecraft were located during the event (also see Movie S2). The footpoints of the spacecraft L shells trace to the same local times where the convection is observed. During 15:00-16:00 UT, peak L-o-S velocities of ∼1000 m/s were also observed at 9-15 MLT region (Figure S4) by radars at higher (68-76°) latitudes. Later on the day, between 19:00-21:30 UT, enhanced L-o-S velocities of about >1250 m/s is measured by radars at higher latitudes (68-76°) in 9-12 and 15-21 MLT regions. During this interval, both spacecraft were orbiting very close to the Earth (perigee) near morning side and hence did not observe any EMIC wave or injection signatures. Further, after 21:20 UT, as both probes advance to their apogees in the dusk sector, VAP-A following VAP-B, wave activities are observed on both probes. No significant (> 750 m/s) plasma convection signatures were observed during this later (>21:30 UT) intervals.

In this study, SuperDARN measurements are used to identify the convection instead of Van Allen Probes electric field measurements. This is because the spacecraft will only give in-situ local electric field values rather than the global convection measurement which are required for the present study. However, electric field measurements from Van Allen Probes' EFW instrument (Wygant et al., 2013) were also examined which show

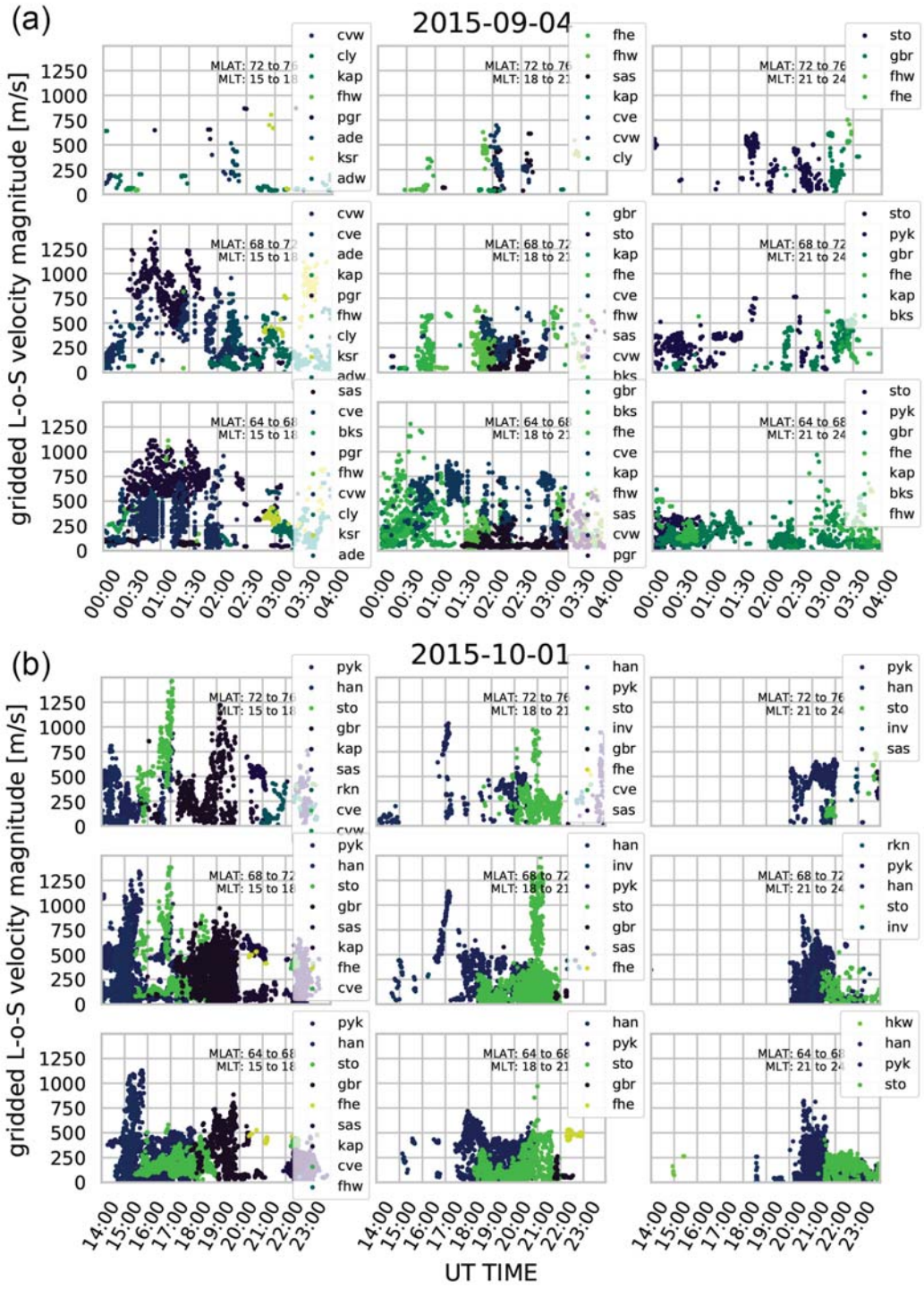

Figure 4. Gridded L-o-S velocity magnitude for the duration (a) 00:00-04:00 UT on 04 September 2015 and (b) 14:00-24:00 UT on 01 October 2015. Each panel shows combined measurements from radars (shown in the legend) whose field of view scans the 4° MLAT and 3 hours MLT bin as shown on top right corner in each panel.

enhanced in-situ electric fields and consequently enhanced magnetospheric convection during the EMIC event intervals (not shown).

3 Summary and Conclusions

Enhanced convection during substorms has been reported by several studies in the past, for example, Freeman et al. (1992); Pellinen (1993); Lester et al. (1996); Förster et al. (2006); Tanaka (2007); Milan et al. (2019) and references therein. The present study reports observations indicating an association between EMIC wave enhancements and enhanced convection periods during substorm injections. We presented examples of EMIC wave events triggered by ion injections during two substorms. The two substorm events are identified using injection signatures observed at geosynchronous orbit as well as at the Van Allen Probes. The SuperMAG list of substorms also identifies substorm onset times which are found to match well with the observed injection signatures in the events. Not all the official substorm onset times correspond to ion flux increases at Van Allen Probes, perhaps because the spacecraft were not in the appropriate locations to see some injections. Every flux increase observed at geosynchronous orbits or at Van Allen Probes during both events corresponded very closely to EMIC wave activity enhancements. During these events we observed enhanced ionospheric plasma flow velocities which indicate strong magnetospheric convection. Our observations are similar to the statistical results by Hwang et al. (2007) who found an association of enhanced convection periods with dawnside chorus wave activity excited by the substorm-injected electrons. A statistical study is now warranted.

Our preliminary survey suggest that injections associated with strong EMIC waves are associated with clear enhanced convection. This could be due to two possible reasons: (i) injections associated with strong convections are stronger with higher ion fluxes and/or (ii) stronger convection increases temperature anisotropy leading to conditions that favor wave growth. Here, the initial look suggests that stronger convection leads to stronger or higher flux injections and the EMIC wave onsets match with the arrival times of increased hot ion flux. Our initial survey also suggests that injections without EMIC waves are associated with little or no convection. However, more work is needed in this direction. We further need to test the statistical significance of our results using more number of events. Noted that the present study deals with substorms during non-storm time periods and in the absence of solar wind pressure pulses. It will be an interesting future work to look at the nature of the correlation between magnetospheric waves and ionospheric convections for various geomagnetic conditions.

Acknowledgments

The Van Allen Probes EMFISIS data are available at http://emfisis.physics.uiowa.edu/, HOPE data at https://rbsp-ect.lanl.gov/ and RBSPICE data at http://rbspice.ftecs.com/Data.html. Processing and analysis of the HOPE data was supported by Energetic Particle, Composition, and Thermal Plasma (RBSP-ECT) investigation funded under NASA's Prime contract no. NAS5-01072. The authors thank Craig Kletzing for the EMFISIS data. We gratefully acknowledge the SuperMAG collaborators (http://supermag.jhuapl.edu/info/?page=acknowledgement). The authors acknowledge the use of SuperDARN data. SuperDARN is a collection of radars funded by national scientific funding agencies of Australia, Canada, China, France, Italy, Japan, Norway, South Africa, United Kingdom and the United States of America. The authors acknowledge access to the SuperDARN database via the Virginia Tech SuperDARN group and their website (http://vt.superdarn.org/). We acknowledge use of NASA/GSFC's Space Physics Data Facility's OMNI/CDAWeb for solar wind parameters and geomagnetic indices. The LANL satellite energetic particle data are provided by Geoff Reeves. Portions of this research were funded by the Van Allen Probes mission.

B. Kunduri thanks and acknowledges the support of NSF under grants AGS-1822056 and AGS-1839509.

References

Anderson, B. J., & Hamilton, D. C. (1993). Electromagnetic ion cyclotron waves stimulated by modest magnetospheric compressions. *J. Geophys. Res. Space Physics*, *98*, 11369-11382. doi: 10.1029/93JA00605

Axford, W. I. (1969). Magnetospheric convection. *Rev. Geophys.*, *7*(1,2), 421-459. doi: 10.1029/RG007i001p00421

Baker, D. N., Higbie, P. R., Hones, J. E. W., & Belian, R. D. (1978). High-resolution energetic particle measurements at 6.6 re 3. low-energy electron anisotropies and short-term substorm predictions. *Journal of Geophysical Research*, *83*, 4863-4868. doi: 10.1029/JA083iA10p04863

Birn, J., Thomsen, M. F., Borovsky, J. E., Reeves, G. D., McComas, D. J., & Belian, R. D. (1997). Characteristic plasma properties during dispersionless substorm injections at geosynchronous orbit. *Journal of Geophysical Research*, *102*(A2), 2309-2324. doi: 10.1029/96JA02870

Borovsky, J. E., Nemzek, R. J., & Belian, R. D. (1993). The occurrence rate of magnetosphericsubstorm onsets: Random and periodic substorms. *J. Geophys. Res.*, *98*(A3), 3807-3813. doi: 10.1029/92JA02556

Chisham, G., Lester, M., Milan, S. E., Freeman, M. P., Bristow, W. A., Grocott, A., ... Walker, A. D. M. (2007). A decade of the super dual auroral radar network (superdarn): scientific achievements, new techniques and future directions. *Surv. Geophys.*, *28*(1), 33-109. doi: 10.1007/s10712-007-9017-8

Cornwall, J. M. (1965). Cyclotron instabilities and electromagnetic emission in the ultra low frequency and very low frequency ranges. *J. Geophys. Res.*, *70*(1), 61-69. doi: 10.1029/JZ070i001p00061

Cornwall, J. M., & Schulz, M. (1971). Electromagnetic ion-cyclotron instabilities in multicomponent magnetospheric plasmas. *J. Geophys. Res.*, *76*, 7791-7796. doi: 10.1029/JA076i031p07791

Cowley, S. W. H., & Lockwood, M. (1992). Excitation and decay of solar wind-driven flows in the magnetosphere-ionophere system. *Ann. Geophys.*, *10*, 103-115. doi: 1992AnGeo..10..103C

Denton, M. H., Henderson, M. G., Jordanova, V. K., Thomsen, M. F., Borovsky, J. E., Woodroffe, J., ... Pitchford, D. (2016). An improved empirical model of electron and ion fluxes at geosynchronous orbit based on upstream solar wind conditions. *Space Weather*, *14*, 511-523. doi: 10.1002/2016SW001409

Dungey, J. W. (1961). Interplanetary magnetic field and the auroral zones. *Phys. Rev. Lett.*, *6*(2), 47-48. doi: 10.1103/PhysRevLett.6.47

Engebretson, M. J., Lessard, M. R., Bortnik, J., Green, J. C., Horne, R. B., Detrick, D. L., ... Rose, M. C. (2008). Pc1-Pc2 waves and energetic particle precipitation during and after magnetic storms: Superposed epoch analysis and case studies. *J. Geophys. Res.*, *113*. (A01211) doi: 10.1029/2007JA012362

Engebretson, M. J., Posch, J. L., Wygant, J. R., Kletzing, C. A., Lessard, M. R., Huang, C.-L., ... Shiokawa, K. (2015). Van Allen probes, NOAA, GOES, and ground observations of an intense EMIC wave event extending over 12 h in magnetic local time. *J. Geophys. Res. Space Physics*, *120*, 5465–5488. doi: 10.1002/2015JA021227

Erlandson, R. E., & Ukhorskiy, A. J. (2001). Observations of electromagnetic ion cyclotron waves during geomagnetic storms: Wave occurrence and pitch angle scattering. *J. Geophys. Res.*, *106*(A3), 3883-3895. doi: 10.1029/2000JA000083

Förster, M., Mishin, V., Stauning, P., Watermann, J., Saifudinova, T., & Bazarzhapov, A. (2006). Plasma convection in the earth's magnetosphere

and ionosphere during substorms. *Adv. Space Res.*, *38*(8), 1750-1754. doi: 10.1016/j.asr.2006.03.029

Freeman, M. P., Southwood, D. J., Lester, M., Yeoman, T. K., & Reeves, G. D. (1992). Substorm-associated radar auroral surges. *J. Geophys. Res.*, *97*(A8), 12173-12185. doi: 10.1029/92JA00697

Funsten, H. O., Skoug, R. M., Guthrie, A. A., MacDonald, E. A., Baldonado, J. R., Harper, R. W., ... Chen, J. (2013). Helium, Oxygen, Proton, and Electron (HOPE) Mass Spectrometer for the Radiation Belt Storm Probes Mission. *Space Science Reviews*, *179*, 1-4. doi: 10.1007/s11214-013-9968-7

Greenwald, R. A., Baker, K. B., Hutchins, R. A., & Hanuis, C. (1985). An hf phased-array radar for studying small-scale structure in the high-latitude ionosphere. *Radio Sci.*, *20*, 63-79. doi: 10.1029/RS020i001p00063

Halford, A. J., Fraser, B. J., & Morley, S. K. (2010). EMIC wave activity during geomagnetic storm and nonstorm periods: CRRES results. *J. Geophys. Res.*, *115*. (A12248) doi: 10.1029/2010JA015716

Halford, A. J., Fraser, B. J., Morley, S. K., Elkington, S. R., & Chan, A. A. (2016). Dependence of EMIC wave parameters during quiet, geomagnetic storm, and geomagnetic storm phase times. *J. Geophys. Res. Space Physics*, *121*, 6277–6291. (A12248) doi: 10.1002/2016JA022694

Hwang, J. A., Lee, D.-Y., Lyons, L. R., Smith, A. J., Zou, S., Min, K. W., ... Park, Y. D. (2007). Statistical significance of association between whistler-mode chorus enhancements and enhanced convection periods during high-speed streams. *J. Geophys. Res.*, *112*, A09213. doi: 10.1029/2007JA012388

Jordanova, V. K., Albert, J., & Miyoshi, Y. (2008). Relativistic electron precipitation by EMIC waves from self-consistent global simulations. *J. Geophys. Res.*, *113*. (A00A10) doi: 10.1029/2008JA013239

Kennel, C. F., & Petschek, H. E. (1966). Limit on stably trapped particle fluxes. *J. Geophys. Res.*, *71*, 1-28. doi: 10.1029/JZ071i001p00001

Khan, H., & Cowley, S. (1999). Observations of the response time of high-latitude ionospheric convection to variations in the interplanetary magnetic field using eiscat and imp-8 data. *Annales Geophysicae*, *17*, 1306-1335. doi: 10.1007/s00585-999-1306-8

Kletzing, C. A., Kurth, W. S., Acuna, M., MacDowall, R. J., Torbert, R. B., Averkamp, T., ... Tyler, J. (2013). The Electric and Magnetic Field Instrument Suite and Integrated Science (EMFISIS) on RBSP. *Space Sci. Rev.*, *179*, 127–181. doi: 10.1007/s11214-013-9993-6

Lee, D.-Y., Lyons, L. R., Kim, K. C., Baek, J.-H., Kim, K.-H., Kim, H.-J., ... Han, W. (2006). Repetitive substorms caused by alfve nic waves of the interplanetary magnetic field during high-speed solar wind streams. *J. Geophys. Res.*, *111*, A12214. doi: 10.1029/2006JA011685

Lester, M., Fox, N. J., Reeves, G. D., & Hairston, M. (1996, October). Ionospheric convection during different phases of magnetospheric substorms. In E. J. Rolfe & B. Kaldeich (Eds.), *International conference on substorms* (Vol. 389, p. 103). doi: 1996ESASP.389..103L

Li, W., Thorne, R. M., Angelopoulos, V., Bortnik, J., Cully, C. M., Ni, B., ... Magnes, W. (2009). Global distribution of whistlermode chorus waves observed on the themis spacecraft. *Geophys. Res. Lett.*, *36*(L09104). doi: 10.1029/2009GL037595

Milan, S. E. (2015). Sun et Lumière: Solar wind-Magnetosphere coupling as deduced from ionospheric flows and polar auroras. In D. Southwood, S. W. H. Cowley, & S. Mitton (Eds.), *Magnetospheric plasma physics: The impact of Jim Dungey's research* (Vol. 41, p. 33-64). Springer International Publishing. doi: 10.1007/978-3-319-18359-6

Milan, S. E., Walach, M.-T., Carter, J. A., Sangha, H., & Anderson, B. J. (2019). Substorm onset latitude and the steadiness of magnetospheric convection. *J.*

Geophys. Res. Space Physics, *124*, 1738-1752. doi: 10.1029/2018JA025969

Mitchell, D. G., Lanzerotti, J., Kim, C. K., Stokes, M., Ho, G., Cooper, S., ... Kerem, S. (2013). Radiation belt storm probes ion composition experiment (rbspice). *Space Sci. Rev.*, *179*, 263-308. doi: 10.1007/s11214-013-9965-x

Newell, P. T., & Gjerloev, J. W. (2011a). Evaluation of supermag auroral electrojet indices as indicators of substorms and auroral power. *J. Geophys. Res.*, *116*, A12211. doi: 10.1029/2011JA016779

Newell, P. T., & Gjerloev, J. W. (2011b). Substorm and magnetosphere characteristic scales inferred from the supermag auroral electrojet indices. *J. Geophys. Res.*, *116*, A12232. doi: 10.1029/2011JA016936

Nishitani, N., Ruohoniemi, J., Lester, M., Baker, J. B. H., Koustov, A. V., Shepherd, S. G., ... Kikuchi, T. (2019). Review of the accomplishments of mid-latitude super dual auroral radar network (superdarn) hf radars. *Progress in Earth and Planetary Science*, *6*(1), 27. doi: 10.1186/s40645-019-0270-5

Olson, J. V., & Lee, L. C. (1983). Pc1 wave generation by sudden impulses. *Planet. Space Sci.*, *31*(3), 295-297. doi: 10.1016/0032-0633(83)90079-X

Park, J.-S., Kim, K.-H., Shiokawa, K., Lee, D.-H., Lee, E., Kwon, H.-J., ... Jee, G. (2016). EMIC waves observed at geosynchronous orbit under quiet geomagnetic conditions (Kp$\leq$1). *J. Geophys. Res. Space Physics*, *121*, 1377–1390. doi: 10.1002/2015JA021968

Pellinen, R. (1993). How does magnetospheric convection relate to the expansion onset of substorms. *J. Atmos. Terr. Phys.*, *55*(8), 1137-1150. doi: 10.1016/0021-9169(93)90042-W

Reeves, G., Belian, R., Cayton, T., Christensen, R., Henderson, M., & McLachlan, P. (1996, October). Los Alamos space weather data products: on line and on time. In E. Rolfe & B. Kaldeich (Eds.), *International conference on substorms* (Vol. 389, p. 689).

Remya, B., Sibeck, D. G., Halford, A. J., Murphy, K. R., Reeves, G. D., Singer, H. J., ... Thaller, S. A. (2018). Ion injection triggered emic waves in the earth's magnetosphere. *J. Geophys. Res. Space Physics*, *123*, 4921-4938. doi: 10.1029/2018JA025354

Rossberg, L. (1984). A close look at the solar wind-magnetosphere interaction. *J. Geophys. Res.*, *89*(A4), 2162-2168. doi: 10.1029/JA089iA04p02162

Ruohoniemi, J., & Baker, K. B. (1998). Large-scale imaging of high-latitude convection with super dual auroral radar network hf radar observations. *J. Geophys. Res.*, *103*(A9), 20797-20811. doi: 10.1029/98JA01288

Ruohoniemi, J., & Greenwald, R. A. (1998). The response of high-latitude convection to a sudden southward imf turning. *Geophys. Res. Lett.*, *25*(15), 2913-2916. doi: 10.1029/98GL02212

Ruohoniemi, J., Greenwald, R. A., Baker, K. B., Villain, J. P., & McCready, M. A. (1987). Drift motions of smallscale irregularities in the highlatitude f region: An experimental comparison with plasma drift motions. *J. Geophys. Res.*, *92*(A5), 4553– 4564. doi: 10.1029/JA092iA05p04553

Ruohoniemi, J., Shepherd, S., & Greenwald, R. (2002). The response of the high-latitude ionosphere to imf variations. *J. Atmos. Sol.-Terr. Phys.*, *64*(2), 159-171. doi: 10.1016/S1364-6826(01)00081-5

Shepherd, S. G., Greenwald, R. A., & Ruohoniemi, J. M. (1999). A possible explanation for rapid, large-scale ionospheric responses to southward turnings of the imf. *Geophys. Res. Lett.*, *26*(20), 3197-3200. doi: 10.1029/1999GL010670

Spence, H., Reeves, G., Baker, D., Blake, J., Bolton, M., Bourdarie, S., ... Thorne, R. (2013). Science goals and overview of the Radiation Belt Storm Probes (RBSP) Energetic particle, Composition, and Thermal plasma (ECT) suite on NASA's Van Allen Probes Mission. *Space Sci. Rev.*, *179*, 311–336. doi: 10.1007/s11214-013-0007-5

Tanaka, T. (2007). Magnetosphere–ionosphere convection as a compound system.

Space Sci. Rev., *133*, 1-72. doi: 10.1007/s11214-007-9168-4

Thorne, R. M., & Kennel, C. F. (1971). Relativistic electron precipitation during magnetic storm main phase. *J. Geophys. Res.*, *76*(19), 4446-4453. doi: 10.1029/JA076i019p04446

Wang, D., Yuan, Z., Yu, X., Huang, S., Deng, X., Zhou, M., & Li, H. (2016). Geomagnetic storms and EMIC waves: Van Allen Probe observations. *J. Geophys. Res. Space Physics*, *121*, 6444-6457. doi: 10.1002/2015JA022318

Wygant, J., Bonnell, J. W., Goetz, K., & et al. (2013). The Electric Field and Waves Instruments on the Radiation Belt Storm Probes Mission. *Space Sci. Rev.*, *179*, 183-220. doi: 10.1007/s11214-013-0013-7